in vivo *39*: 160-171 (2025)
doi:10.21873/invivo.13814

The Relationship of Metabolic Activity and αvβ3 Receptor Expression in Aggressive Breast Cancer Subtypes Tumors: A Preliminary Report

TOÀN MINH NGÔ[1,2], TAMÁS NAGY[2,3], ZOLTÁN SZOBOSZLAI[3], CSABA CSIKOS[1,2], NOÉMI DÉNES[2], ANDREA FURKA[4], GYÖRGY TRENCSÉNYI[1,2#] and ILDIKÓ GARAI[1,2,3#]

[1]*Gyula Petrányi Doctoral School of Clinical Immunology and Allergology, Faculty of Medicine, University of Debrecen, Debrecen, Hungary;*
[2]*Division of Nuclear Medicine and Translational Imaging, Department of Medical Imaging, University of Debrecen, Debrecen, Hungary;*
[3]*Scanomed Ltd., Debrecen, Hungary;*
[4]*Department of Oncology, University of Debrecen, Debrecen, Hungary*

Abstract. *Background/Aim: Angiogenesis imaging has been a valuable complement to metabolic imaging with 2-deoxy-2-[^{18}F]fluoroglucose (FDG). In our longitudinal study, we investigated the tumour heterogeneity and the relationship between FDG and [^{68}Ga]Ga-NODAGA-c(RGDfK)$_2$ (RGD) accumulation in breast cancer xenografts. Materials and Methods: Two groups of cell lines, a fast-growing (4T1) and a slow-growing cell line (MDA-MB-HER2+), were inoculated into SCID mice. RGD and FDG scans were performed in all mice on separate days at four time points. Assessment of tumour uptake based on positron emission tomography/magnetic resonance imaging images was performed using tumour/muscle ratios with the Muscle-Spacing Correction Method to minimize the partial volume effect of the urinary bladder. Results: In the 4T1 group, both radiopharmaceuticals visualized the highly heterogeneous structure of the tumours and showed correlations with tumour growth. Relative linear correlations between FDG and RGD tumour/muscle ratios were observed in all tumours, evident in both high and low-activity areas of 4T1 tumours. When comparing the two groups of different cell lines, SUV ratios in the 4T1 group were higher, especially with [^{18}F]F-FDG. Our findings highlight the correlations between FDG and RGD, particularly in aggressive breast cancer. Conclusion: This preliminary study supports the combined use of FDG and RGD PET imaging to better characterize tumor heterogeneity and aggressiveness in breast cancer. The observed correlation between FDG and RGD uptake offers insights into the metabolic and vascular behavior of different cancer subtypes, highlighting distinct patterns in 4T1 and MDA-MB-HER2+ lines. This dual-tracer approach shows promise for tailoring therapies based on tumor subtype, though further studies with larger samples are needed to validate these initial findings.*

The rapid development of positron emission tomography (PET) imaging provides an opportunity to investigate the heterogeneity of both inter-tumor and intra-tumor characteristics, particularly in conjunction with high-resolution anatomical references from computed tomography (CT) or magnetic resonance imaging (MRI) images. These hybrid modalities have already demonstrated their clinical utility through routine [^{18}F]F-FDG (2-deoxy-2-[^{18}F]fluoroglucose) (FDG) scans for cancer staging or follow-up and have become an essential aspect of cancer management.

In general, an elevated FDG uptake is indicative of more active or aggressive cancers and consequently have worse prognosis (1). However, FDG uptake is dependent on many complex molecular mechanisms that involve both cancer cells and their microenvironment. These include processes, such as tumor cell metabolism, vascularization, and supporting stromal cell activity (2).

#These Authors contributed equally to this study.

Correspondence to: Toàn Minh Ngô, Nagyerdei krt. 98, Debrecen H-4032, Hungary. Tel: +36 304771176, e-mail: ngo@mailbox.unideb.hu

Key Words: FDG, RGD, breast cancer, PET imaging, angiogenesis imaging.

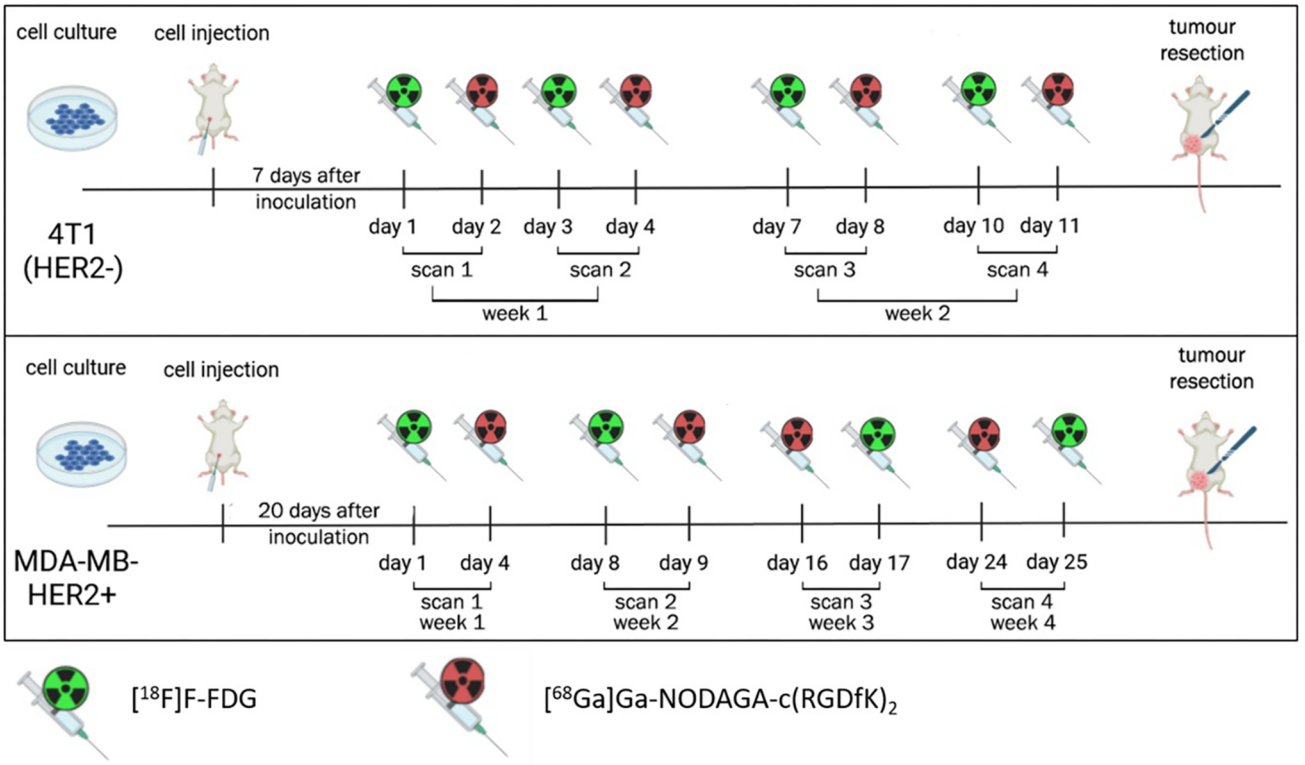

Figure 1. *Timeline of the study including cell culturing, tumor inoculation, and scanning time of the fast-growing cell line 4T1 (upper) and of the slow-growing cell line MDA-MB-HER2+ (lower).*

Angiogenesis is well-known to play a vital role in disease progression. The process involves the production of new blood vessels through endothelial proliferation, which is a cellular activity driven by various signaling factors arising from tumor cells and their surrounding microenvironment. *Via* these newly formed blood vessels, angiogenesis directly facilitates tumor growth and enhances the invasive capabilities of tumor cells (3).

Recently, many anti-angiogenic therapies have demonstrated the ability to inhibit tumor growth, invasion, and metastasis (4). A key component in this process is integrin αvβ3 which significantly contributes to tumor progression, particularly in promoting angiogenesis. Consequently, targeting αvβ3 has emerged as an attractive strategy for anti-angiogenic therapy. While many peptide-based agents targeting αvβ3 have shown limited effectiveness due to partial agonist effects and changes in affinity of the receptors, various alternative strategies including allosteric modulators or pure antagonists have been developed to enhance the efficacy of αvβ3-targeted treatments. These innovative approaches have demonstrated promising results and are being translated into clinical studies (5). Moreover, integrin αvβ3 up-regulates PD-L1 expression in the tumor microenvironment, indicating that its inhibition could facilitate the checkpoint inhibitors therapy (6, 7). Additionally, due to its angiogenic effects at low doses, integrin αvβ3 therapy has been shown to enhance chemotherapy delivery and efficacy in preclinical tumor-bearing models (8).

Nevertheless, targeting αvβ3 for *in vivo* angiogenesis imaging is another promising approach being studied. Assessing cancer angiogenesis could be beneficial before initiating anti-angiogenic therapy and follow-up treatments. By integrating angiogenesis imaging with FDG PET, we can gain valuable insights into the intricate relationship between cancer metabolism and angiogenesis in various cancer types. Numerous radiopharmaceuticals have been developed due to the over-expression of this heterodimeric integrin on the surface of tumour endothelial cells (9). Arginine-glycine-aspartic acid (RGD)-based radiopharmaceuticals, particularly cyclic pentapeptides like RGDfK, have demonstrated high specificity for visualizing αvβ3. Polymerizing these peptides, especially in a dimeric form, has yielded promising and consistent results (10). Therefore, in our study, we selected [^{68}Ga]Ga-NODAGA-c(RGDfK)$_2$ (RGD) as the radiopharmaceutical of choice for targeting cancer angiogenesis.

Thanks to the relatively short biological and physical half-lives of [^{18}F]F-FDG and [^{68}Ga]-c(RGDfK)$_2$ ($T_{1/2}$ ^{18}F=109.7 minutes, $T_{1/2}$ ^{68}Ga=68 minutes) (11), we were able to perform a longitudinal study using dual radiopharmaceuticals to closely monitor tumour progression.

In this study, we investigated the relationship between the tumour over muscle ratios of [^{68}Ga]Ga-NODAGA-c(RGDfK)$_2$ and [^{18}F]F-FDG of the xenograft and their relationship with tumour growth. Changes in activity over time were investigated in two different cell lines inoculated in preclinical models: 4T1, a fast-growing triple-negative murine breast cancer cell line; and a slow-growing MDA-MB-HER2+ (HER2-positive) human breast cancer cell line. These represent the most aggressive breast cancer subtypes with the worst long-term overall survival rate under conventional therapies (12). Additionally, tumour heterogeneity within the fast-growing 4T1 tumour was assessed.

Materials and Methods

Radiopharmaceuticals. NODAGA-c(RGDfK)$_2$ was obtained from ABX (Radeberg, Germany). Ultrapure HCl, NH4OAc buffer and water were purchased from Merck KGaA (Darmstadt, Germany). Oasis HLB 1 cc cartridge was the product of Waters Corporation (Milford, MA, USA). All other reagents and solvents were obtained from Sigma-Aldrich Ltd. (Budapest, Hungary) and were of analytical grade. They were used without further purification in all cases.

[^{18}F]F-FDG was produced following the Good Manufacturing Practice (GMP) standards for its clinical use in PET imaging. [^{18}F]F-FDG production was performed in the radiochemical laboratory of the Division of Nuclear Medicine and Translational Imaging, Department of Medical Imaging, Faculty of Medicine, University of Debrecen (Debrecen, Hungary).

Cyclotron produced ^{68}Ga (Division of Nuclear Medicine and Translational Imaging, Department of Medical Imaging, University of Debrecen, Hungary) was used for radiolabeling NODAGA-c(RGDfK)$_2$. After fractional elution, 0.5 ml eluate was buffered with 0.5 ml (3 mol/dm^3) ultrapure ammonium acetate to adjust the pH of the reaction mixture to 4-4.1 for each compound. A 10 µl (3 mmol/dm^3) NODAGA-RGD dimer acetate aq. solution was added, and the reaction solution was incubated for 15 min at 95˚C. Then, solid-phase extraction (SPE – Waters Oasis HLB cartridge; 30 mg) was required to trap the radiopeptide. The radiolabeled peptide ([^{68}Ga]Ga-NODAGA-c(RGDfK)$_2$) was elutable from the HLB column with 0.1 ml of isotonic NaCl solution/EtOH 1:1 mixture. [^{68}Ga]Ga-NODAGA-c(RGDfK)$_2$ was produced with a high specific activity (15.7±0.17 GBq/µmol) and a good radiochemical purity (>95%), in all cases. Quality control of the radiolabeled NODAGA-c(RGDfK)$_2$ was performed with thin-layer chromatography and citrate buffer was used as an eluent (0.1 mol/dm^3; pH=5.5).

Cell lines and preclinical models. Cell lines were generously provided by Dr. György Vereb (Department of Biophysics and Cell Biology, University of Debrecen). They were cultured at 37˚C with 5% CO_2 in Dulbecco's Modified Eagle Medium (DMEM, GIBCO, Life Technologies Magyarország Ltd., Budapest, Hungary), supplemented with 10% fetal bovine serum (FBS) (10%, heat-inactivated FBS from GIBCO, Life technologies) and 1% antibiotic-antimycotic solution (1%, Sigma-Aldrich, Merck KGaA, Darmstadt, Germany). Monolayer cultures were passaged three times a week.

Female CB17 SCID mice, weighing 21.68±2.74 g and between ages of 12 to 16 weeks, were divided into two groups: one group of mice (n=2, limited number of sample due to the death of mice during the protocol) was inoculated with a fast-growing cell line (4T1), whereas the other group (n=3) received a slow-growing tumor cell line (MDA-MB-HER2+). Ethical approval for the animal research was obtained from the Ethical Committee for Animal Research at the University of Debrecen, Hungary, under permission number 8/2016/DEMÁB. Compliance with all relevant Hungarian laws and European Union animal welfare guidelines, following the "4R" principles (reduce, refine, replace, and responsibility), was ensured in animal handling.

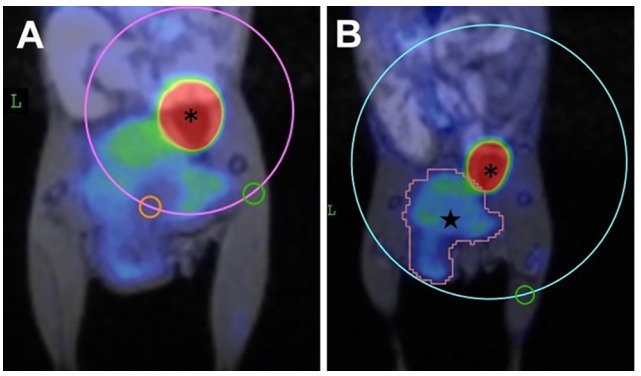

Figure 2. *Muscle-Spacing Correction Method: To guarantee the equal distance from the urinary bladder to each measured volume of interest (VOI), a large VOI is drawn over the center of the urinary bladder. This bladder VOI intersects with both the central point of the tumor's avid/non-avid area VOI/the furthest point of the whole tumor VOI from the bladder and the center of the reference muscle VOI. (A) Evaluating tumor heterogeneity, pink circle denotes the urinary bladder VOI, orange circle indicates the non-avid area VOI, green circle represents the muscle reference VOI, and the asterisk sign indicates the urinary bladder. (B) Accessing the whole tumor uptake; light blue circle indicates the urinary bladder VOI, the brown VOI indicates the whole tumor VOI, and the green circle represents the muscle reference VOI; the asterisk marks the urinary bladder.*

4T1 cells and MDA-MB-HER2+ cells were injected into the fat pad of the inguinal breast at a concentration of 5×10^6 cells in saline (150 µl 0.9% NaCl) to achieve optimal xenograft growth (13). For a complete xenograft establishment, imaging was started two days after tumor onset (when tumors were first detected and palpable): 7 days and 20 days after inoculation of 4T1 (14) and MDA-MB-HER2+ cell lines, respectively (Figure 1).

In vivo experimental protocol. Both the groups received FDG and RGD four times on separate days. In the 4T1 group, mice were scanned four times in two weeks with both tracers, whereas the HER2-positive group underwent weekly scans for four weeks (Figure 1).

Administration of the radiopharmaceuticals into the lateral tail veins was carried out under inhalational anesthesia. The acquisition occurred after an incubation period, allowing sufficient time for urinary excretion to minimize urinary bladder uptake. The exact injected radioactivity was determined by measuring the syringe volume and calculating the activity using a dose calibrator before and after every injection.

The administered dose of [^{18}F]F-FDG was 14.83±2.91 MBq. Prior to scanning, mice were subjected to overnight fasting, lasting for at least 12 h, to minimize background uptake in the blood pool and myocardium. The incubation time before scanning was 80.45±2.47 min.

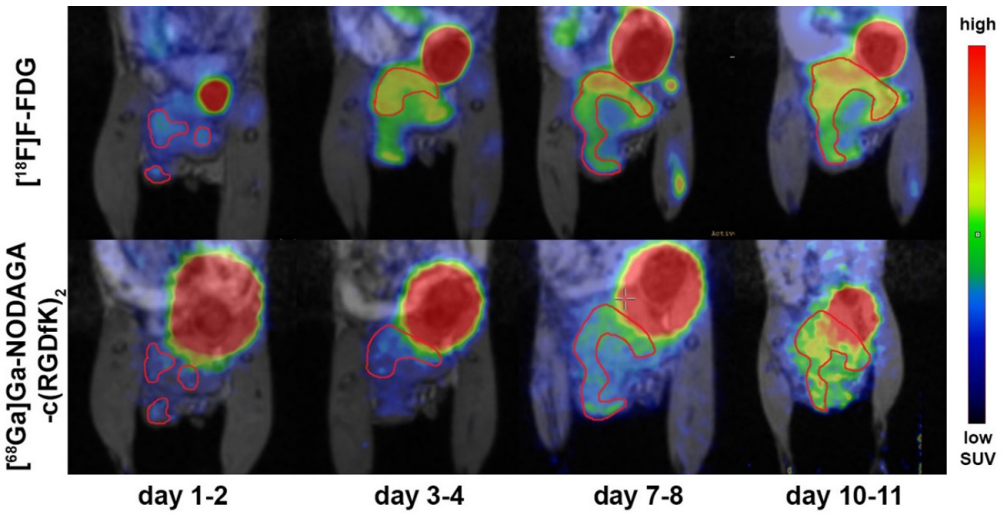

Figure 3. *PET/MRI hybrid images on different scanning days using [^{18}F]F-FDG (upper row) and [^{68}Ga]Ga-NODAGA-c(RGDfK)$_2$ (lower row) on 4T1 tumor-bearing mouse. Red contours highlight the avid areas within the tumor. The SUV scale is displayed at the right.*

The administered dose of [^{68}Ga]Ga-NODAGA-c(RGDfK)$_2$ was 14.45±3.83 MBq. All mice were provided with a sterile semi-synthetic rodent diet and sterile tap water before the scan. The incubation time before scanning was 82.95±5.27 min.

In vivo imaging protocol. PET/MRI images were conducted using the nanoScan® PET/MRI 1T (Mediso Ltd., Budapest, Hungary) while ensuring the animals remained under inhalational anesthesia with isoflurane (Forane, AbbVie, Budapest, Hungary) (3% for initiation and 2% for maintenance) with a continuous supply of 0.4 l/min oxygen (Linde Healthcare, Budapest, Hungary) and 1.2 l/min nitrous oxide gas (Linde Healthcare). The animals were securely positioned on a scanning bed to maintain a constant body temperature of 37°C throughout the procedure.

PET acquisitions lasted for 20 min with a field of view (FOV) of 98.5 mm. Following the PET scan, MRI acquisition was performed with specific parameters: flip angle of 20 degrees, repetition time of 15 ms, echo time of 2 ms, FOV of 60 mm, and number of excitations was set to 2, for approximately 18 min.

Reconstruction of the acquired raw data was carried out using Nucline software (Mediso Ltd.) and employed the 3D-OSEM (Ordered Subset Expectation Maximization) algorithm with attenuation correction and random correction. When reconstructing [^{18}F]F-FDG images, the voxel size was set at 0.4 mm^3 with 6 iterations and low regularization. In contrast, the reconstruction of [^{68}Ga]Ga-NODAGA-c(RGDfK)$_2$ images utilized a smaller voxel size of 0.3 mm^3, 12 iterations, and high regularization to enhance resolution and minimize partial volume effects, which is more pronounced when imaging with ^{68}Ga due to its higher positron energy of 1.9 MeV (11).

In vivo PET measurements. Measurements were done with InterView™ FUSION software (Mediso Ltd.). Volume-of-interests (VOIs) were delineated on both tumor and muscle reference areas using Muscle-Spacing Correction Method, *i.e.,* using muscle reference with an equal distance from the urinary bladder to correct its spillover effect (Figure 2).

To assess tumor heterogeneity, VOIs with a diameter of 2 mm were drawn over the most avid and least avid regions within the tumor. These VOIs were positioned equidistant with the reference VOIs from the center of the urinary bladder to minimize the partial volume effect of the bladder activity (Figure 2A).

Activity of the entire tumor was assessed by drawing VOIs manually around the tumor's contour. Muscle uptake was used as a reference, and the distance from the bladder to the reference muscle was adjusted to match the distance of the farthest point of the tumor from the bladder (Figure 2B).

To calculate the Standardized Uptake Value (SUV) the following formula was used: SUV=[VOI activity (MBq/ml)]/[injected activity (MBq)/animal weight (g)]. Evaluation of tumor uptake was performed by calculating the ratio of tumor SUV_{mean} to muscle SUV_{mean}.

Regions of interest (ROIs) were drawn around the tumor contours in each axial slice of the MRI images. Tumor volumes were calculated by summing the areas of these ROIs and multiplying the result by the slice thickness (0.5 mm).

Histopathology and immunohistochemistry. After the last scan, the mice were euthanized, and the tumors were resected, fixed in 10% formalin and frozen at a fixed temperature of –20°C. The tumors were then sent for histopathologic and immunohistochemistry examinations. In addition to the conventional hematoxylin and eosin (H&E) staining, immunohistochemistry staining was performed to visualize the expression of GLUT1 transporter (GLUT1 Recombinant Rabbit Monoclonal Antibody, SA0377, Thermo Fisher Scientific, Dreieich, Germany) and avb3 integrin (Anti-Integrin αVβ3 Antibody, clone EM22703 ZooMAb® Rabbit Monoclonal, Merck KGaA) proteins. Texas-red (Goat anti-Rabbit IgG (H+L) Cross-Adsorbed Secondary Antibody, Texas Red, Thermo Fisher Scientific) was used as the secondary antibody, and cell nuclei were counterstained with DAPI (DAPI ready-made solution, MBD0015, Merck KGaA).

Data presentation. Due to the small sample size, resulting in a non-normal distribution, data were presented as median and interquartile range: median (lower quartile to upper quartile). All the graphs were created using GraphPad Prism 9.4.1 software (GraphPad Software, Boston, MA, USA).

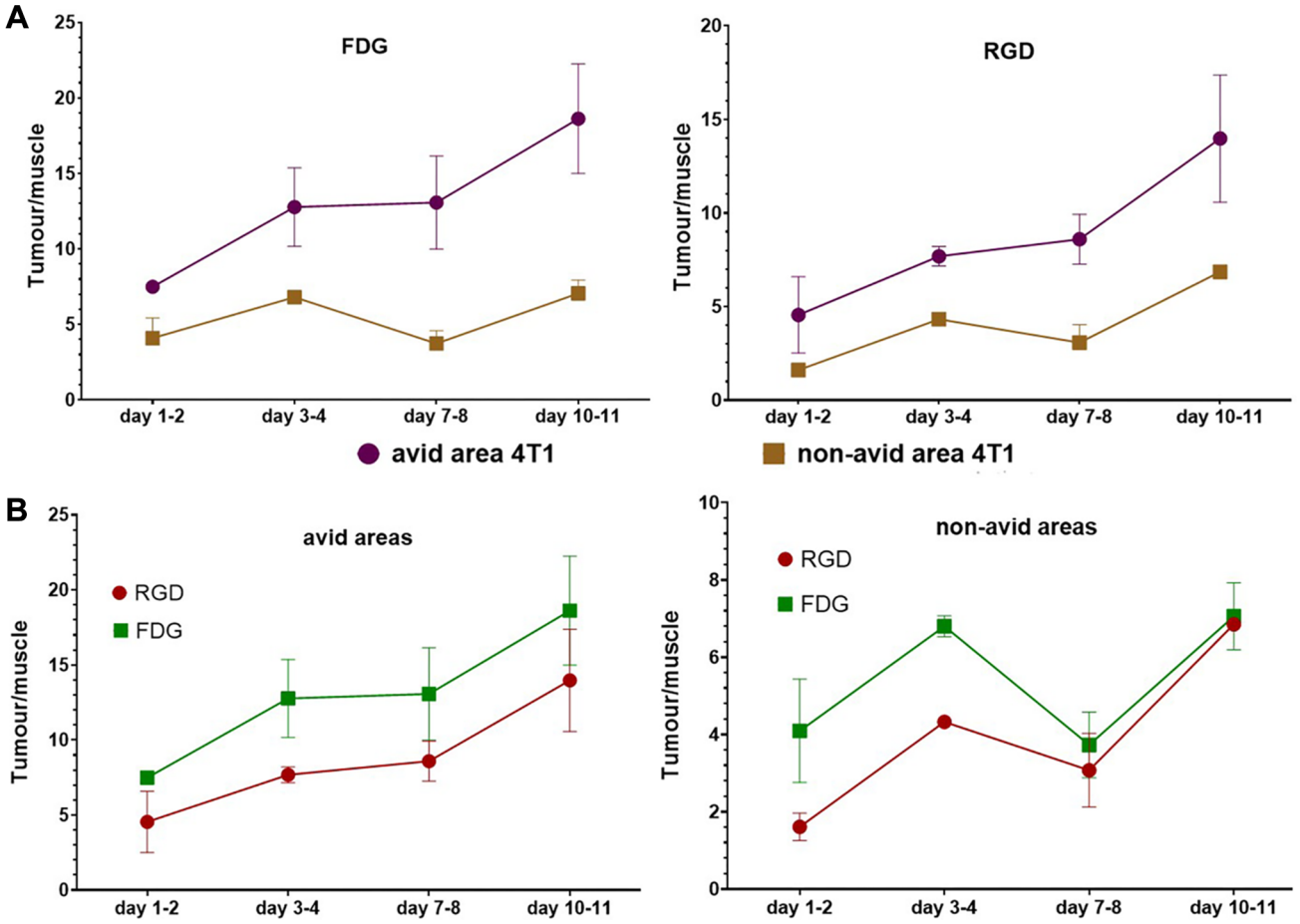

Figure 4. *Line graphs presenting tumor/muscle ratios using [^{18}F]F-FDG (FDG) and [^{68}Ga]Ga-NODAGA-c(RGDfK)$_2$ (RGD) in avid areas and non-avid areas of 4T1 tumors (A, B).*

Results

4T1 tumor heterogeneity. During our two-week longitudinal study, there was significant heterogeneity in the tracer uptake in different areas within the 4T1 tumors. We monitored the changes in the activities of both high-uptake areas (avid areas) and low-uptake areas (non-avid areas) throughout the study (Figure 3). Based on SUV measurements, there were fluctuations in tumor/muscle ratios in both radiopharmaceuticals. As the tumors grew, the heterogeneity became more prominent (on days 7-8 and days 10-11). These differences were more pronounced when using [^{18}F]F-FDG compared to [^{68}Ga]Ga-NODAGA-c(RGDfK)$_2$. Specifically, the ratios of [^{18}F]F-FDG uptakes on days 10-11 were: avid areas 18.62 (14.99 to 22.25) *vs*. non-avid areas 7.06 (6.19 to 7.93); whereas with [^{68}Ga]Ga-NODAGA-c(RGDfK)$_2$ the ratios were: avid areas 13.98 (10.58 to 17.38) *vs*. non-avid areas 6.85 (6.74 to 6.97) (Figure 4A).

Tracking the changes of the two tracers over time in both avid and non-avid areas revealed a synchronized pattern (Figure 4B).

4T1 and MDA-MB-HER2+ whole tumor assessment. Due to the noticeable trends between FDG and RGD in both avid and non-avid areas of fast-growing 4T1 tumors, we investigated the correlation across the entire tumor. Based on the line graphs following the two tracers over time, it was evident that the two ratios were comparable, and their changes follow a similar direction. The scatter plot further confirmed this observation, revealing a relatively remarkable positive correlation between the two tracers, which both increased from the 1st scan [FDG: 7.22 (7.00 to 7.43), RGD: 9.05 (6.13 to 11.96)] to the 3rd scan [FDG: 9.05 (9.03 to 9.06), RGD: 12.63 (10.48 to 14.79)] (Figure 5A). Furthermore, HER2-positive graph also revealed a relative correlation in this slow-growing group, even though the correlation seemed weaker. Specifically, there was a slight increase in FDG from week 1: 2.04 (1.50 to 2.39) to week 2: 2.04 (1.74 to 2.015), and week 3: 2.45 (1.32 to 4.21), whereas the RGD decreased from week 1: 8.70 (7.76 to 9.93) to week 2: 7.50 (4.98 to 10.37), and week 3: 5.35 (5.26 to 25.88). Nevertheless, scatter plots revealed a

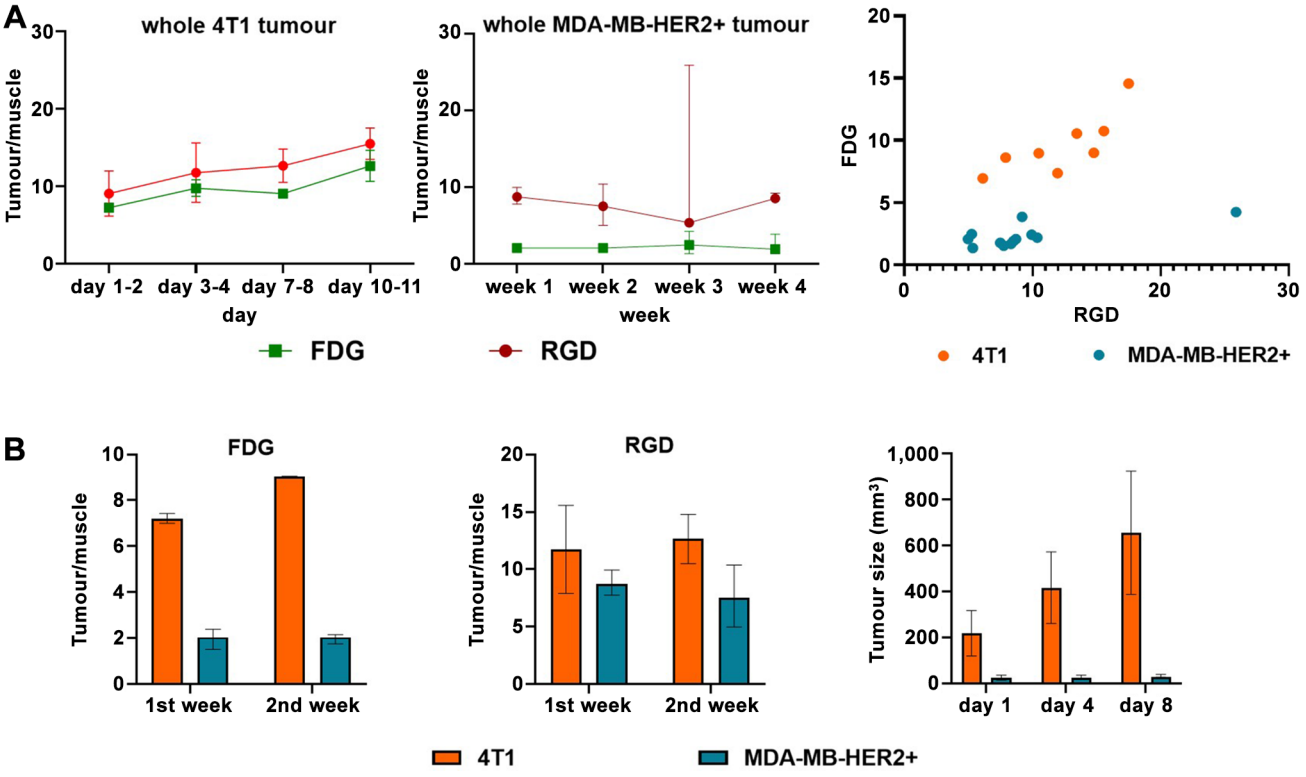

Figure 5. *Line graphs and scatter plots of whole tumor/muscle ratios using [^{18}F]F-FDG and [^{68}Ga]Ga-NODAGA-c(RGDfK)$_2$ in MDA-MB-HER2+ tumors and 4T1 tumors (A). Bar graphs demonstrate the tumor/muscle ratios using [^{18}F]F-FDG (left), [^{68}Ga]Ga-NODAGA-c(RGDfK)$_2$ (middle) in the 1st (day 1: FDG, day 4: RGD) and 2nd (day 7-8: FDG, day 8-9: RGD) scanning week on MDA-MB-HER2+ and 4T1 tumors, right bar graph compares tumor sizes of the two groups (B).*

noticeable correlation between the two tracers in both groups (Figure 5A).

However, there was a noticeable difference in the trend of whole tumor FDG ratios over RGD ratios between 4T1 and MDA-MB-HER2+ xenografts. The MDA-MB-HER2+ tumors exhibited higher tumor-to-muscle ratios for RGD compared to FDG, resulting in notably lower FDG-to-RGD ratios in this group, as demonstrated in the scatter plot (Figure 5A).

There were notable differences in tumor sizes within the two groups, *i.e.*, on day 8: MDA-MB-HER2+ tumor size was 28.84 (27.97 to 39.98) mm^3, whereas 4T1 tumor size was 656.24 (387.81 to 924.66) mm^3 (Figure 5B). When comparing the FDG SUV_{mean} ratios between the two groups on corresponding scanning days, consistently higher ratios were observed in the fast-growing 4T1 group. For instance, in the second week, the FDG ratio for 4T1 tumors was 9.05 (9.03 to 9.06), while for MDA-MB-HER2+ tumors, it was 2.04 (1.74 to 2.15). The difference was less pronounced for the RGD tracer (the ratios of 4T1 tumor *vs.* MDA-MB-HER2+ tumor on the second week were 12.63 [10.48 to 14.79) *vs.* 7.50 (4.98 to 10.37), respectively] (Figure 5B).

There were notable correlations between FDG ratios and RGD ratios with the tumor sizes in the 4T1 group. Both line graphs (Figure 6A) and scatter plots (Figure 6B) demonstrated comparable positive correlations between 4T1 tumor sizes and 4T1 tumor-to-muscle ratios using the two radiopharmaceuticals. However, these positive correlations were not as visible in the slow-growing group (Figure 7).

Histopathology and immunohistochemistry examination. H&E staining revealed that the triple-negative tumor group was stroma-rich, while the HER2-positive group showed prominent necrosis. GLUT1 transporter staining in the 4T1 xenografts showed strong, widespread staining, particularly in the stromal areas. HER2-positive tumors had less intense GLUT1 transporter staining, which showed a rather heterogeneous cellular distribution. The two tumor types displayed similar αvβ3 integrin staining intensities, with HER2-positive tumors showing slightly weaker stromal staining and a more uniform distribution (Figure 8).

Discussion

The results of our study show a noticeable positive correlation between glucose metabolism and angiogenesis imaging, indicating their possible significant interplay in

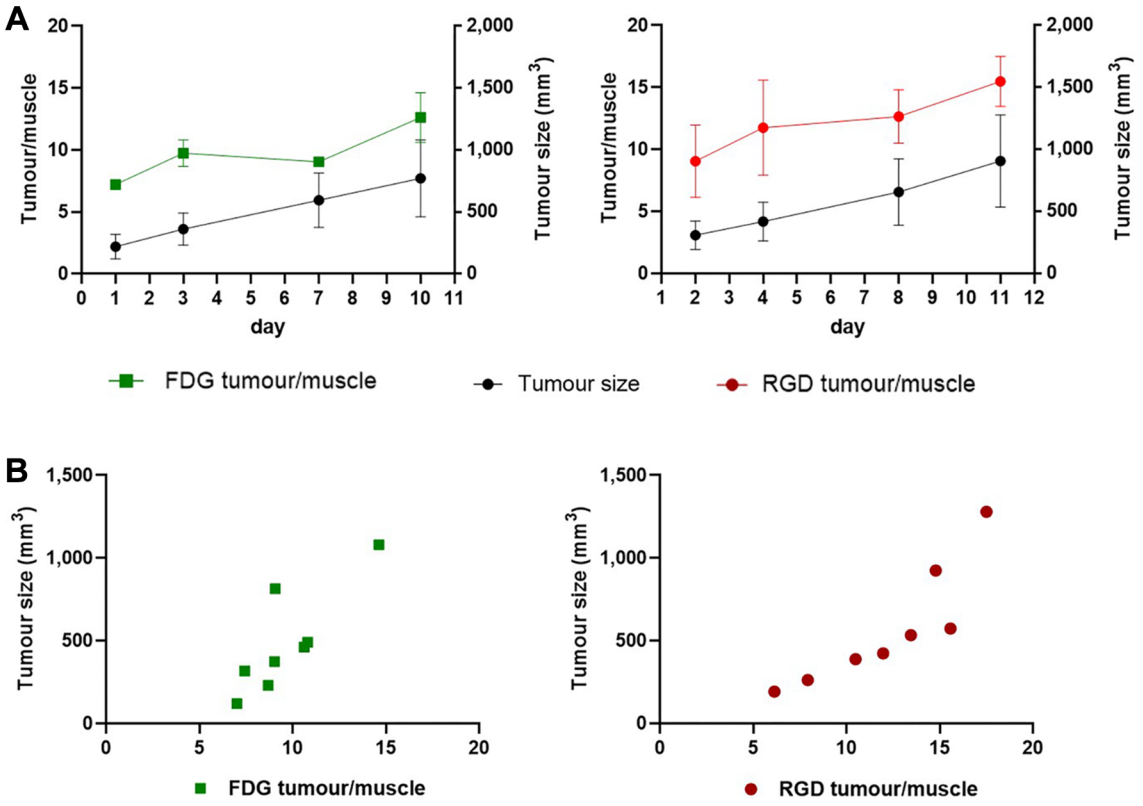

Figure 6. *Line graphs (A) and scatter plots (B) showing changes over time and correlation between tumor sizes and whole tumor/muscle* SUV_{mean} *ratios using [*^{18}*F]F-FDG (left) and [*^{68}*Ga]Ga-NODAGA-c(RGDfK)*$_2$ *(right) in 4T1 tumors.*

tumor characterization. Moreover, both FDG and RGD correlate with tumor growth, particularly in the 4T1 tumor. Furthermore, there were variations in FDG over RGD ratios between the two groups, highlighting the different behaviors among breast cancer subtypes.

Angiogenesis relies on several biochemical processes, which include the expression of pro-angiogenetic factors, VEGF, bFGF, TGF, TNF, and other cytokines and growth factors, especially under hypoxic conditions mediated *via* the transcription factor HIF-1α. In addition, inhibiting negative regulatory processes, such as tissue inhibitor metalloprotease, angiotensin, and angiostatin, is also required for effective angiogenesis (3). Therefore, considering the substantial energy demands of intercellular crosstalk within the cancer microenvironment, there may be a direct correlation between angiogenesis and glucose utilization.

Studies have indeed demonstrated a positive correlation of FDG uptake with different histologic angiogenesis markers, such as CD31 and CD105, in lung and breast cancers (15-17), prompting ongoing investigations into the relationship between FDG and RGD tracers. Wei *et al*. conducted a study on mice bearing lung cancer xenografts and found a very strong correlation between these two tracers with r=0.917 (18). Additionally, several clinical studies have reported a positive correlation across various tumor types, particularly in tumors with high FDG avidity (rectal, breast, non-small cell lung cancer, and head and neck cancer) (19-27). The correlation between the two radiopharmaceuticals may become more evident when their values are corrected using a muscle reference (21, 27). This adjustment is necessary due to the substantially lower uptake of RGD compared to FDG in general (21, 27-29) and the distinct differences in the biodistribution of these two radiopharmaceuticals (30).

In our study, relatively positive linear correlations were observed between RGD and FDG tumor/muscle ratios regardless of the growth rate of the tumor, indicating a potentially significant relationship between angiogenesis and glucose metabolism. It is assumed that several factors may contribute to these observations. Firstly, tumor endothelial cells were found to up-regulate glucose transporters GLUT1 and GLUT3 in response to high glucose transportation (31) leading to increased FDG uptake in regions of enhanced angiogenesis. Additionally, cancer cells exhibit an elevated FDG uptake due to the Warburg effect, particularly within hypoxic regions (32). These hypoxic areas are closely associated with regions undergoing angiogenesis, further

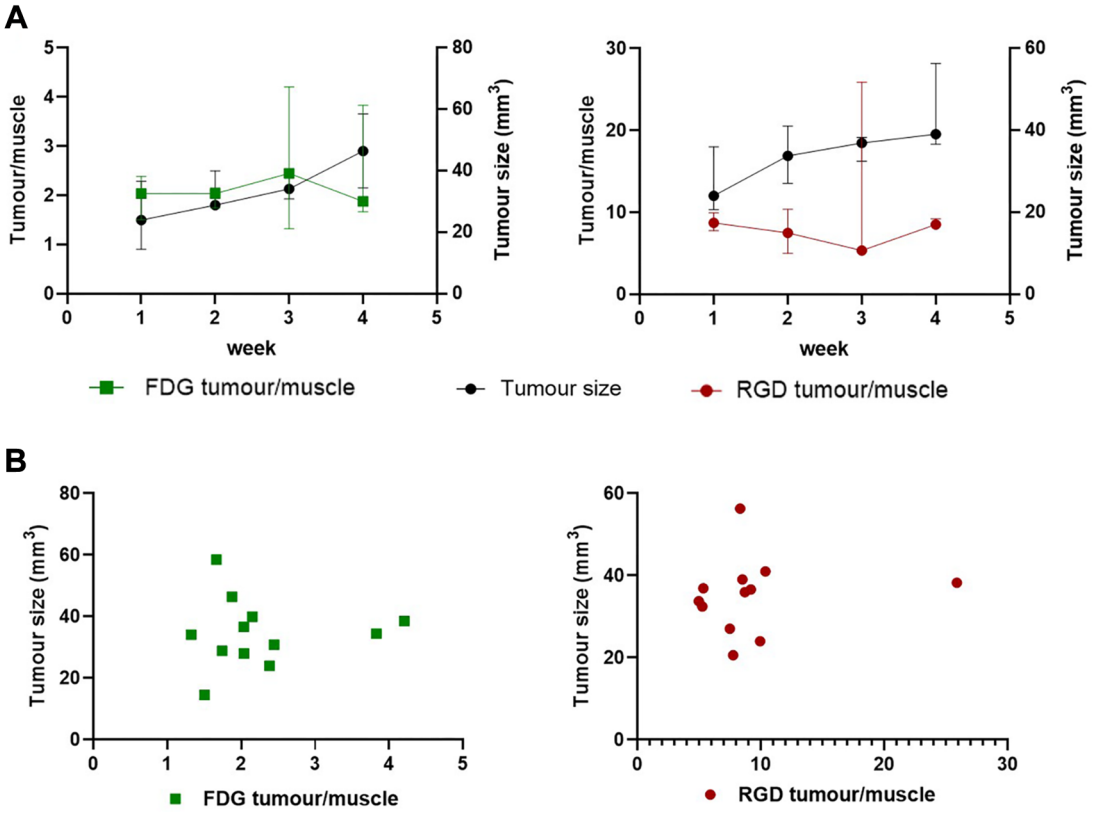

Figure 7. *Line graphs (A) and scatter plots (B) showing changes over time and correlation between tumor sizes and whole tumor/muscle* SUV_{mean} *ratios using [*^{18}*F]F-FDG (left) and [*^{68}*Ga]Ga-NODAGA-c(RGDfK)*$_2$ *(right) in MDA-MB-HER2+ tumors.*

contributing to the strong correlation between FDG uptake and angiogenic regions (33). Moreover, cancer-associated fibroblasts have a significant impact on tumor FDG uptake (34), and have an essential role in angiogenesis processes, particularly in cancers with substantial stromal components, such as breast cancers (35). Furthermore, angiogenesis in cancer is characterized by abnormal vessel formation involving immature endothelial cells which tend to be leaky, and lack proper basement membrane and supporting pericytes (36). This neo-vasculature is associated with increased permeability and perfusion within the tumor (37), further enhancing FDG uptake (38).

Utilizing the observed correlation between tumor sizes and tumor/muscle SUV ratios of the two tracers, coupled with the ability to assess tumor heterogeneity, provides a valuable means of precisely determining the target tumor volume for therapy. In our study, comparable correlations of the FDG and RGD with tumor size were observed, especially in the aggressive tumors. The correlations were not clearly seen in slow-growing tumors, likely due to the different behaviors between subtypes of the same cancer, as reported in a study on non-small cell lung cancer, where both adenocarcinoma and squamous cell carcinoma demonstrated positive correlations between FDG uptake and tumor size; however, the correlation coefficient and correlation pattern varied between the two subtypes (39). Nevertheless, comparing the correlation of two tracers with tumor size, a previous larger study reported a superior correlation of RGD with the pathologic volume of the tumor (40), possibly because tumor growth heavily relies on angiogenesis more linearly, while glucose metabolism is more complex, encompassing elements like inflammation and stromal activity. RGD imaging can assist oncology surgeons to determine the possible resection margins or even delineate the gross tumor volume for radiotherapy by precise detection of the tumor extension. Therefore, it can serve as a specific predictive tool, minimizing false positives associated with inflammation, for evaluating tumor progression and monitoring responses to treatment, particularly in anti-angiogenic therapy (41, 42) used in metastatic colorectal cancer, non-small-cell lung cancer, glioblastoma, ovarian and cervical cancers (43).

Despite differences in growth rates, the breast cancer subtypes used in our study represent the most aggressive types reliant on angiogenesis, resulting in the highest expression of αvβ3 among all breast cancer subtypes (44, 45). While both cell lines exhibited correlations in tumor/muscle ratios between FDG and RGD, glucose metabolism was noticeably

higher than angiogenesis in the 4T1 triple-negative cell line. This observation can be attributed to the aggressive nature of 4T1, given that the triple-negative breast cancer subtype is known to have the worst prognosis and the lowest survival rate of all breast cancer subtypes regardless of cancer stage (46, 47). Consequently, this aggressive subtype, displaying a faster growth rate, has a higher FDG-to-RGD ratio when compared to other subtypes (25). Furthermore, larger tumors are associated with denser microvascularity, which facilitates the penetration and uptake of FDG, thus increasing overall FDG tumor uptake (38). Our histopathological examination revealed that 4T1 had an abundant tumor stroma, which has been reported in the literature (48). The stroma-rich cancer environment has a significant impact on increased FDG uptake within the tumor, especially in cancers with high FDG that have a greater distribution of stroma (34). In contrast, the HER2-positive subtype is known to have the highest rate of parenchymal organ metastases among all breast cancer subtypes (49), although recent advances in HER2-targeted therapies have improved the survival rates of this particular subtype. As a result, HER2-enriched tumors displayed an elevated RGD uptake, whereas triple-negative breast cancer exhibited lower RGD uptake relative to its high FDG uptake (25, 50). Moreover, a study has associated HER2 positivity with an increased expression of HIF-1α (51), which may further promote neo-angiogenesis (33). These explain the minimal differences observed between the HER2-positive xenograft and the aggressive triple-negative 4T1 xenograft when using RGD imaging and αvβ3 integrin staining.

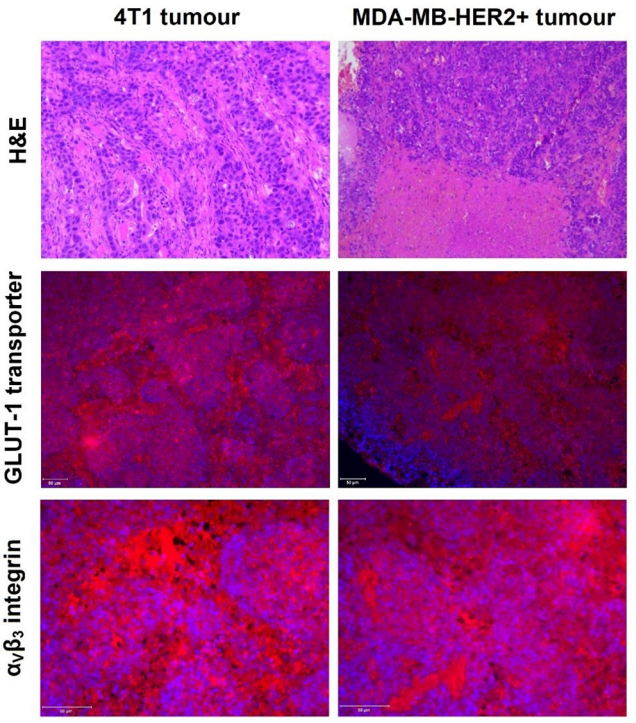

Figure 8. *Histopathology and immunohistochemistry results of triple-negative (4T1) and HER2 positive (MDA-MB-HER2+) xenografts. Upper row shows hematoxylin and eosin (H&E) staining, middle row and bottom row display GLUT-1 transporter and αvβ3 integrin staining, respectively.*

Tumors characterized by a higher FDG uptake (22) or higher FDG tumor-to-muscle ratio, like the triple-negative breast cancer subtype we used in our experiments, exhibited a more robust correlation between neo-angiogenesis and FDG-avidity in comparison to other tumors (25, 52). Our study observed relatively more linear relationships in the group with higher FDG tumor-to-muscle ratios; however, due to the small sample size no statistical analysis was performed to investigate the differences further, thus the results should be considered preliminary. Nevertheless, this observation emphasizes the significance of neo-angiogenesis in tumor growth, particularly in aggressive tumors, where rapid growth demands high levels of oxygen and nutrients.

Peptide-derived tracers like RGD are predominantly excreted *via* the kidneys, leading to high activity accumulation in the urinary bladder (53). This can cause a partial volume effect, resulting in false increased activity measured in the surrounding organs. Invasive bladder continuous flushing (54) and non-invasive hydration plus furosemide (55) protocols have been proposed to minimize this artifact. Reconstructing with spatial resolution improvements, such as using the Ordered Subset Expectation Maximization (OSEM) iterative reconstruction method (54), increasing the number of iterations, and reducing voxel size (56), have been attempted to reduce this unwanted effect. In this study, we further enhanced quantitative accuracy without *in vivo* intervention by implementing the Muscle-Spacing Correction Method. Taking advantage of the consistently minimal muscular uptake, along with the homogenous and relatively oval shape of the fully filled urinary bladder, the method uses a muscle VOI as the reference for background correction. In order to ensure equal distances from the reference VOI to the bladder center and from the target VOI to the bladder center, an additional VOI is drawn. Its center aligns with the center of the bladder and intersects with the centers of the target and reference VOIs. Utilizing this method, we can correct the partial volume effect not only when the target is near the bladder but also potentially in brain imaging, where a similar phenomenon frequently occurs.

One notable limitation of this study is the relatively small sample size, especially in the 4T1 group (n=2), which may limit the statistical power and the generalizability of the findings. Additionally, the measuring method employed in the study has not been thoroughly validated, and therefore further investigation is needed to verify the reliability and reproducibility of the technique. Moreover, it is important to acknowledge that breast cancers are substantially complex and heterogeneous with various subtypes exhibiting distinct

molecular profiles and clinical behaviors. Further research with larger sample sizes and various breast cancer subtypes is necessary to confirm the complex relationship between glucose metabolism, vascular formation, and tumor progression in this heterogeneous cancer type.

Conclusion

In conclusion, our preliminary report emphasizes the possible strong correlation between glucose metabolism and angiogenesis imaging, revealing their complex roles in tumor characterization. Accumulation of FDG and RGD exhibit a substantial relationship with tumor growth, emphasizing RGD's potential in clinical applications. Additionally, the observed variations in the ratio between FDG and RGD reflect the diverse behaviors among breast cancer subtypes. Due to the small number of subjects in this preliminary report, a larger study is needed to provide more robust evidence for the findings, especially across all breast cancer subtypes.

Funding

This research received no external funding.

Conflicts of Interest

The Authors declare no conflicts of interest in relation to this study.

Authors' Contributions

Conceptualization and methodology, I.G., T.M.N., and G.T.; preclinical models handling, T.N., T.M.N.; Z.S. quality control; radiopharmaceutical labelling N.D.; investigation, T.M.N.; writing—original draft preparation, N.M.T.; review and editing, G.T., I.G., C.C., A.F. All Authors have read and agreed to the published version of the manuscript.

References

1 Huang Y, Feng M, He Q, Yin J, Xu P, Jiang Q, Lang J: Prognostic value of pretreatment 18F-FDG PET-CT for nasopharyngeal carcinoma patients. Medicine (Baltimore) 96(17): e6721, 2017. DOI: 10.1097/MD.0000000000006721

2 Peppicelli S, Andreucci E, Ruzzolini J, Bianchini F, Calorini L: FDG uptake in cancer: a continuing debate. Theranostics 10(7): 2944-2948, 2020. DOI: 10.7150/thno.40599

3 Nishida N, Yano H, Nishida T, Kamura T, Kojiro M: Angiogenesis in cancer. Vasc Health Risk Manag 2(3): 213-219, 2006. DOI: 10.2147/vhrm.2006.2.3.213

4 Lopes-Coelho F, Martins F, Pereira SA, Serpa J: Anti-angiogenic therapy: current challenges and future perspectives. Int J Mol Sci 22(7): 3765, 2021. DOI: 10.3390/ijms22073765

5 Gu Y, Dong B, He X, Qiu Z, Zhang J, Zhang M, Liu H, Pang X, Cui Y: The challenges and opportunities of αvβ3-based therapeutics in cancer: From bench to clinical trials. Pharmacol Res 189: 106694, 2023. DOI: 10.1016/j.phrs.2023.106694

6 Slack RJ, Macdonald SJF, Roper JA, Jenkins RG, Hatley RJD: Emerging therapeutic opportunities for integrin inhibitors. Nat Rev Drug Discov 21(1): 60-78, 2022. DOI: 10.1038/s41573-021-00284-4

7 Pan X, Yi M, Liu C, Jin Y, Liu B, Hu G, Yuan X: Cilengitide, an αvβ3-integrin inhibitor, enhances the efficacy of anti-programmed cell death-1 therapy in a murine melanoma model. Bioengineered 13(2): 4557-4572, 2022. DOI: 10.1080/21655979.2022.2029236

8 Wong PP, Demircioglu F, Ghazaly E, Alrawashdeh W, Stratford MR, Scudamore CL, Cereser B, Crnogorac-Jurcevic T, McDonald S, Elia G, Hagemann T, Kocher HM, Hodivala-Dilke KM: Dual-action combination therapy enhances angiogenesis while reducing tumor growth and spread. Cancer Cell 27(1): 123-137, 2015. DOI: 10.1016/j.ccell.2014.10.015

9 Danhier F, Le Breton A, Préat V: RGD-based strategies to target Alpha(v) Beta(3) integrin in cancer therapy and diagnosis. Mol Pharmaceut 9(11): 2961-2973, 2012. DOI: 10.1021/mp3002733

10 Liolios C, Sachpekidis C, Kolocouris A, Dimitrakopoulou-Strauss A, Bouziotis P: PET diagnostic molecules utilizing multimeric cyclic RGD peptide analogs for imaging integrin α(v)β(3) receptors. Molecules 26(6): 1792, 2021. DOI: 10.3390/molecules26061792

11 Nolting DD, Nickels ML, Guo N, Pham W: Molecular imaging probe development: A chemistry perspective. Am J Nucl Med Mol Imaging 2(3): 273-306, 2012.

12 Yang SX, Polley EC: Systemic treatment and radiotherapy, breast cancer subtypes, and survival after long-term clinical follow-up. Breast Cancer Res Treat 175(2): 287-295, 2019. DOI: 10.1007/s10549-019-05142-x

13 Okano M, Oshi M, Butash A, Okano I, Saito K, Kawaguchi T, Nagahashi M, Kono K, Ohtake T, Takabe K: Orthotopic implantation achieves better engraftment and faster growth than subcutaneous implantation in breast cancer patient-derived xenografts. J Mammary Gland Biol Neoplasia 25(1): 27-36, 2020. DOI: 10.1007/s10911-020-09442-7

14 Gregório AC, Fonseca NA, Moura V, Lacerda M, Figueiredo P, Simões S, Dias S, Moreira JN: Inoculated cell density as a determinant factor of the growth dynamics and metastatic efficiency of a breast cancer murine model. PLoS One 11(11): e0165817, 2016. DOI: 10.1371/journal.pone.0165817

15 Porter JC, Ganeshan B, Win T, Fraioli F, Khan S, Rodriguez-Justo M, Endozo R, Shortman RI, Hoy LR, Maher TM, Groves AM: [(18)F]FDG PET/CT signal correlates with neoangiogenesis markers in patients with fibrotic interstitial lung disease who underwent lung biopsy: implication for the use of PET/CT in diffuse lung diseases. J Nucl Med 65(4): 617-622, 2024. DOI: 10.2967/jnumed.123.266445

16 Mirus M, Tokalov SV, Abramyuk A, Heinold J, Prochnow V, Zöphel K, Kotzerke J, Abolmaali N: Noninvasive assessment and quantification of tumor vascularization using [18F]FDG-PET/CT and CE-CT in a tumor model with modifiable angiogenesis-an animal experimental prospective cohort study. EJNMMI Res 9(1): 55, 2019. DOI: 10.1186/s13550-019-0502-0

17 Groves AM, Shastry M, Rodriguez-Justo M, Malhotra A, Endozo R, Davidson T, Kelleher T, Miles KA, Ell PJ, Keshtgar MR: ^{18}F-FDG PET and biomarkers for tumour angiogenesis in early breast cancer. Eur J Nucl Med Mol Imaging 38(1): 46-52, 2011. DOI: 10.1007/s00259-010-1590-2

18 Wei YC, Gao Y, Zhang J, Fu Z, Zheng J, Liu N, Hu X, Hou W, Yu J, Yuan S: Stereotactic comparison study of (18)F-Alfatide and (18)F-FDG PET imaging in an LLC tumor-bearing C57BL/6 mouse model. Sci Rep 6: 28757, 2016. DOI: 10.1038/srep28757

19 Durante S, Dunet V, Gorostidi F, Mitsakis P, Schaefer N, Delage J, Prior JO: Head and neck tumors angiogenesis imaging with (68)Ga-NODAGA-RGD in comparison to (18)F-FDG PET/CT: a pilot study. EJNMMI Res 10(1): 47, 2020. DOI: 10.1186/s13550-020-00638-w

20 Minamimoto R, Karam A, Jamali M, Barkhodari A, Gambhir SS, Dorigo O, Iagaru A: Pilot prospective evaluation of 18F-FPPRGD2 PET/CT in patients with cervical and ovarian cancer. Eur J Nucl Med Mol Imaging 43(6): 1047-1055, 2016. DOI: 10.1007/s00259-015-3263-7

21 Dietz M, Dunet V, Mantziari S, Pomoni A, Dias Correia R, Testart Dardel N, Boughdad S, Nicod Lalonde M, Treglia G, Schafer M, Schaefer N, Prior JO: Comparison of integrin α(v)β(3) expression with (68)Ga-NODAGA-RGD PET/CT and glucose metabolism with (18)F-FDG PET/CT in esophageal or gastroesophageal junction cancers. Eur J Hybrid Imaging 7(1): 3, 2023. DOI: 10.1186/s41824-023-00162-9

22 Beer AJ, Lorenzen S, Metz S, Herrmann K, Watzlowik P, Wester HJ, Peschel C, Lordick F, Schwaiger M: Comparison of integrin $\alpha_v\beta_3$ expression and glucose metabolism in primary and metastatic lesions in cancer patients: a PET study using ^{18}F-Galacto-RGD and ^{18}F-FDG. J Nucl Med 49(1): 22-29, 2008. DOI: 10.2967/jnumed.107.045864

23 Chen SH, Wang HM, Lin CY, Chang JT, Hsieh CH, Liao CT, Kang CJ, Yang LY, Yen TC: RGD-K5 PET/CT in patients with advanced head and neck cancer treated with concurrent chemoradiotherapy: Results from a pilot study. Eur J Nucl Med Mol Imaging 43(9): 1621-1629, 2016. DOI: 10.1007/s00259-016-3345-1

24 Withofs N, Martinive P, Vanderick J, Bletard N, Scagnol I, Mievis F, Giacomelli F, Coucke P, Delvenne P, Cataldo D, Gambhir SS, Hustinx R: [18F]FPRGD2 PET/CT imaging of integrin αvβ3 levels in patients with locally advanced rectal carcinoma. Eur J Nucl Med Mol Imaging 43(4): 654-662, 2016. DOI: 10.1007/s00259-015-3219-y

25 Yoon HJ, Kang KW, Chun IK, Cho N, Im SA, Jeong S, Lee S, Jung KC, Lee YS, Jeong JM, Lee DS, Chung JK, Moon WK: Correlation of breast cancer subtypes, based on estrogen receptor, progesterone receptor, and HER2, with functional imaging parameters from 68Ga-RGD PET/CT and 18F-FDG PET/CT. Eur J Nucl Med Mol Imaging 41(8): 1534-1543, 2014. DOI: 10.1007/s00259-014-2744-4

26 Ahangari S, Littrup Andersen F, Liv Hansen N, Jakobi Nøttrup T, Berthelsen AK, Folsted Kallehauge J, Richter Vogelius I, Kjaer A, Espe Hansen A, Fischer BM: Multi-parametric PET/MRI for enhanced tumor characterization of patients with cervical cancer. Eur J Hybrid Imaging 6(1): 7, 2022. DOI: 10.1186/s41824-022-00129-2

27 Toriihara A, Duan H, Thompson HM, Park S, Hatami N, Baratto L, Fan AC, Iagaru A: 18F-FPPRGD2 PET/CT in patients with metastatic renal cell cancer. Eur J Nucl Med Mol Imaging 46(7): 1518-1523, 2019. DOI: 10.1007/s00259-019-04295-7

28 Li L, Chen X, Yu J, Yuan S: Preliminary clinical application of RGD-containing peptides as PET radiotracers for imaging tumors. Front Oncol 12: 837952, 2022. DOI: 10.3389/fonc.2022.837952

29 Zheng K, Liang N, Zhang J, Lang L, Zhang W, Li S, Zhao J, Niu G, Li F, Zhu Z, Chen X: 68Ga-NOTA-PRGD2 PET/CT for integrin imaging in patients with lung cancer. J Nucl Med 56(12): 1823-1827, 2015. DOI: 10.2967/jnumed.115.160648

30 Novy Z, Stepankova J, Hola M, Flasarova D, Popper M, Petrik M: Preclinical evaluation of radiolabeled peptides for PET imaging of glioblastoma multiforme. Molecules 24(13): 2496, 2019. DOI: 10.3390/molecules24132496

31 Du W, Ren L, Hamblin MH, Fan Y: Endothelial cell glucose metabolism and angiogenesis. Biomedicines 9(2): 147, 2021. DOI: 10.3390/biomedicines9020147

32 Li XF, Du Y, Ma Y, Postel GC, Civelek AC: (18)F-fluorodeoxyglucose uptake and tumor hypoxia: revisit (18)f-fluorodeoxyglucose in oncology application. Transl Oncol 7(2): 240-247, 2014. DOI: 10.1016/j.tranon.2014.02.010

33 Kis A, Szabó JP, Dénes N, Vágner A, Nagy G, Garai I, Fekete A, Szikra D, Hajdu I, Matolay O, Méhes G, Mező G, Kertész I, Trencsényi G: *In vivo* imaging of hypoxia and neoangiogenesis in experimental syngeneic hepatocellular carcinoma tumor model using positron emission tomography. Biomed Res Int 2020: 4952372, 2020. DOI: 10.1155/2020/4952372

34 Shangguan C, Gan G, Zhang J, Wu J, Miao Y, Zhang M, Li B, Mi J: Cancer-associated fibroblasts enhance tumor (18)F-FDG uptake and contribute to the intratumor heterogeneity of PET-CT. Theranostics 8(5): 1376-1388, 2018. DOI: 10.7150/thno.22717

35 Tripathi M, Billet S, Bhowmick NA: Understanding the role of stromal fibroblasts in cancer progression. Cell Adh Migr 6(3): 231-235, 2012. DOI: 10.4161/cam.20419

36 Tong RT, Boucher Y, Kozin SV, Winkler F, Hicklin DJ, Jain RK: Vascular normalization by vascular endothelial growth factor receptor 2 blockade induces a pressure gradient across the vasculature and improves drug penetration in tumors. Cancer Research 64(11): 3731-3736, 2004. DOI: 10.1158/0008-5472.Can-04-0074

37 Børresen B, Hansen AE, Fliedner FP, Henriksen JR, Elema DR, Brandt-Larsen M, Kristensen LK, Kristensen AT, Andresen TL, Kjær A: Noninvasive molecular imaging of the enhanced permeability and retention effect by (64)Cu-liposomes: *In vivo* correlations with (68)Ga-RGD, fluid pressure, diffusivity and (18)F-FDG. Int J Nanomedicine 15: 8571-8581, 2020. DOI: 10.2147/IJN.S239172

38 Kashkooli FM, Abazari MA, Soltani M, Ghazani MA, Rahmim A: A spatiotemporal multi-scale computational model for FDG PET imaging at different stages of tumor growth and angiogenesis. Sci Rep 12(1): 10062, 2022. DOI: 10.1038/s41598-022-13345-4

39 Karam MB, Doroudinia A, Behzadi B, Mehrian P, Koma AY: Correlation of quantified metabolic activity in nonsmall cell lung cancer with tumor size and tumor pathological characteristics. Medicine (Baltimore) 97(32): e11628, 2018. DOI: 10.1097/MD.0000000000011628

40 Wei YC, Hu X, Gao Y, Fu Z, Zhao W, Yu Q, Wang S, Zhu S, Li J, Yu J, Yuan S: Noninvasive evaluation of metabolic tumor volume in Lewis lung carcinoma tumor-bearing C57BL/6 mice with micro-PET and the radiotracers 18F-Alfatide and 18F-FDG: a comparative analysis. PLoS One 10(9): e0136195, 2015. DOI: 10.1371/journal.pone.0136195

41 Provost C, Rozenblum-Beddok L, Nataf V, Merabtene F, Prignon A, Talbot JN: [^{68}Ga]RGD *versus* [^{18}F]FDG PET imaging in

monitoring treatment response of a mouse model of human glioblastoma tumor with bevacizumab and/or temozolomide. Mol Imaging Biol 21(2): 297-305, 2019. DOI: 10.1007/s11307-018-1224-9

42 Cui Y, Liu H, Liang S, Zhang C, Cheng W, Hai W, Yin B, Wang D: The feasibility of 18F-AlF-NOTA-PRGD2 PET/CT for monitoring early response of Endostar antiangiogenic therapy in human nasopharyngeal carcinoma xenograft model compared with 18F-FDG. Oncotarget 7(19): 27243-27254, 2016. DOI: 10.18632/oncotarget.8402

43 Garcia J, Hurwitz HI, Sandler AB, Miles D, Coleman RL, Deurloo R, Chinot OL: Bevacizumab (Avastin®) in cancer treatment: A review of 15 years of clinical experience and future outlook. Cancer Treat Rev 86: 102017, 2020. DOI: 10.1016/j.ctrv.2020.102017

44 Arslan E, Aksoy T, Can Trabulus FD, Kelten Talu C, Yeni B, Çermik TF: The association of 18F-fluorodeoxyglucose PET/computed tomography parameters with tissue gastrin-releasing peptide receptor and integrin αvβ3 receptor levels in patients with breast cancer. Nucl Med Commun 41(3): 260-268, 2020. DOI: 10.1097/mnm.0000000000001133

45 Chen Z, Fu F, Li F, Zhu Z, Yang Y, Chen X, Jia B, Zheng S, Huang C, Miao W: Comparison of [99mTc]3PRGD2 imaging and [18F]FDG PET/CT in breast cancer and expression of integrin αvβ3 in breast cancer vascular endothelial cells. Mol Imaging Biol 20(5): 846-856, 2018. DOI: 10.1007/s11307-018-1178-y

46 Howlader N, Cronin KA, Kurian AW, Andridge R: Differences in breast cancer survival by molecular subtypes in the United States. Cancer Epidemiol Biomarkers Prev 27(6): 619-626, 2018. DOI: 10.1158/1055-9965.Epi-17-0627

47 Li X, Yang J, Peng L, Sahin AA, Huo L, Ward KC, O'Regan R, Torres MA, Meisel JL: Triple-negative breast cancer has worse overall survival and cause-specific survival than non-triple-negative breast cancer. Breast Cancer Res Treat 161(2): 279-287, 2017. DOI: 10.1007/s10549-016-4059-6

48 Li Q, Li M, Zheng K, Tang S, Ma S: Expression pattern analysis and drug differential sensitivity of cancer-associated fibroblasts in triple-negative breast cancer. Transl Oncol 14(1): 100891, 2021. DOI: 10.1016/j.tranon.2020.100891

49 Kennecke H, Yerushalmi R, Woods R, Cheang MC, Voduc D, Speers CH, Nielsen TO, Gelmon K: Metastatic behavior of breast cancer subtypes. J Clin Oncol 28(20): 3271-3277, 2010. DOI: 10.1200/jco.2009.25.9820

50 Wu J, Zhang X, Jia Z, Zhou X, Qi R, Ji H, Sun J, Sun C, Teng Z, Lu G, Chen X: Combined (18)F-FDG and (18)F-alfatide II PET may predict luminal B (HER2 negative) subtype and nonluminal subtype of invasive breast cancer. Mol Pharm 19(9): 3405-3411, 2022. DOI: 10.1021/acs.molpharmaceut.2c00547

51 Bos R, van der Groep P, Greijer AE, Shvarts A, Meijer S, Pinedo HM, Semenza GL, van Diest PJ, van der Wall E: Levels of hypoxia-inducible factor-1α independently predict prognosis in patients with lymph node negative breast carcinoma. Cancer 97(6): 1573-1581, 2003. DOI: 10.1002/cncr.11246

52 Kaira K, Murakami H, Endo M, Ohde Y, Naito T, Kondo H, Nakajima T, Yamamoto N, Takahashi T: Biological correlation of ^{18}F-FDG uptake on PET in pulmonary neuroendocrine tumors. Anticancer Res 33(10): 4219-4228, 2013.

53 Jahandideh A, Ståhle M, Virta J, Li XG, Liljenbäck H, Moisio O, Knuuti J, Roivainen A, Saraste A: Evaluation of [(68)Ga]Ga-NODAGA-RGD for PET imaging of rat autoimmune myocarditis. Front Med (Lausanne) 8: 783596, 2021. DOI: 10.3389/fmed.2021.783596

54 Deleye S, Heylen M, Deiteren A, De Man J, Stroobants S, De Winter B, Staelens S: Continuous flushing of the bladder in rodents reduces artifacts and improves quantification in molecular imaging. Mol Imaging 13(5): 13, 2014. DOI: 10.2310/7290.2014.00013

55 Cussó L, Desco M: Suppression of 18F-FDG signal in the bladder on small animal PET-CT. PLoS One 13(10): e0205610, 2018. DOI: 10.1371/journal.pone.0205610

56 Zhao J, Liu Q, Li C, Song Y, Zhang Y, Chen JC: Optimization of spatial resolution and image reconstruction parameters for the small-animal Metis™ PET/CT system. Electronics 11(10): 1542, 2022. DOI: 10.3390/electronics11101542

Received September 21, 2024
Revised October 5, 2024
Accepted October 7, 2024